

# Development and characterization of plasma actuators for high-speed jet control

M. Samimy, I. Adamovich, B. Webb, J. Kastner, J. Hileman, S. Keshav, P. Palm

577

**Abstract** Active control of high Reynolds number and high-speed jets has been hampered due to the lack of suitable actuators. Some of the attributes that would make an actuator suitable for such flows are: high amplitude and bandwidth; small size for distribution around the jet; phase-locking ability for jet azimuthal mode forcing; and sufficient ruggedness for hot jets. We have been developing a class of actuators termed ‘localized arc filament plasma actuators,’ which possess such characteristics. In this paper, we present the development and characterization of these actuators as well as preliminary results on their applications in high Reynolds number Mach 0.9 and ideally expanded Mach 1.3 jets.

## 1 Introduction

Manipulation of dynamics of large scale structures in turbulent free jets can be put into two broad categories: (1) direct manipulation of jet instabilities (i.e., initial shear layer and/or jet column instabilities) and (2) imparting longitudinal (streamwise) vortices into the mixing layer of the jet. Both techniques have been successfully used in low-speed and low Reynolds number flows. In contrast, the lack of high amplitude and bandwidth actuators has hampered the use of techniques in the first category in high-speed and high Reynolds number flows; only techniques in the second category have been used successfully for such flows. In the first two sub-sections, a brief overview of some of the relevant work in the literature in both categories will be discussed. The third sub-section will discuss prior work with plasma arcs. The main objective of the current work is to develop, characterize, and use ‘localized arc filament plasma actuators’ (LAFPA) for jet

control. These actuators can potentially be used with either one of the two techniques or a combination of the two techniques in low- or high-speed flows. The focus of the current work is their application in high-speed and high Reynolds number jets.

### 1.1 Shear layer instability manipulation

Over the last few decades, many characteristics of free shear layer instabilities have been studied (e.g., Kibens 1979; Laufer and Yen 1983; Ho and Huerre 1984; Long et al. 1985). Two main instabilities within a jet can be used for jet control: shear layer instability, with its receptivity located at the nozzle exit/trailing edge; and the jet column instability, which is amplified near the end of the potential core. For low Reynolds number jets ( $\sim Re_D < 50,000$ ), acoustic drivers have been successfully used to force the jet. For higher Reynolds number jets, the increased back-ground noise and the high flow momentum have rendered this kind of actuator less effective.

The initial shear layer instability is characterized by a Strouhal number based on the jet’s initial momentum thickness,  $\theta$ ,  $St_\theta = f\theta/U_j$ , where  $U_j$  is the jet exit velocity, and  $f$  is the frequency. While there are some variations in the literature, the maximum *amplification* of disturbances occurs around  $St_\theta = 0.012$  and it is spatially located near the first nonlinear interaction (Michalke 1965). Excitation around  $St_\theta = 0.012$  can lead to an increase in shear layer growth, turbulence intensity, and high amplitude tones in the acoustic far-field with the largest peak at the first subharmonic (Long et al. 1985). On the other hand, the maximum *amplification rate* of disturbances occurs around  $St_\theta = 0.017$ . Since this requires a higher frequency, and a shorter wavelength, energy saturation occurs before the first nonlinear interaction (Zaman and Hussain 1981). When excited at this Strouhal number, the shear layer grows slower in space, has reduced turbulence intensity, and the broadband acoustic energy is decreased. These ideas have been studied in great detail in low Reynolds number jets. However, high Reynolds number jets have not yet been excited at these Strouhal numbers due to the lack of actuators with sufficiently high amplitude and bandwidth—the shear layer instability frequency in a typical small-scale high subsonic jet in a laboratory is in excess of 50 kHz.

Near the end of the potential core, an axisymmetric jet with a low Reynolds number has a preferred axisymmetric mode near a  $St_D = fD/U_j$  of 0.3, where  $D$  is the jet diameter (e.g., Crow and Champagne 1971). There is significant

Received: 5 February 2004 / Accepted: 10 July 2004  
Published online: 18 August 2004  
© Springer-Verlag 2004

M. Samimy (✉), I. Adamovich, B. Webb, J. Kastner, J. Hileman, S. Keshav, P. Palm  
Department of Mechanical Engineering,  
Ohio State University, 43210,  
Columbus, Ohio, US  
E-mail: Samimy.1@osu.edu  
Tel.: +1-614-2926988  
Fax: +1-614-2923163

Patent pending

This work was sponsored by NASA Glenn Research Center under the QAT program (with Drs. Joseph Grady and James Bridges).

variation in the preferred Strouhal number ( $\sim 0.2-0.5$ ), which seems to be facility-dependent (e.g., Gutmark and Ho 1983). When the incoming boundary layer is laminar, the jet column instability amplifies excitation tones only over a narrow band. If the boundary layer is turbulent, the shear layer is able to amplify a broader range of excitation frequencies (Lepicovsky and Brown 1987). Also, with the increased growth of the shear layer downstream, the thickness approaches that of the jet radius, and azimuthal/helical modes are amplified with amplitudes similar to axisymmetric modes (e.g., Cohen and Wygnanski 1987).

Forcing with a combination of axisymmetric and azimuthal modes can enhance mixing by causing the jet to flap, bifurcate, or bloom (Parekh et al. 1996; Kibens et al. 1999; Reynolds et al. 2003). Kibens et al. (1999) used high amplitude pulsed injection to excite the exhaust from a full-scale jet engine at a flapping mode,  $m=\pm 1$  (they used two actuators  $180^\circ$  out of phase, and each covering a quarter of the perimeter of the jet), which resulted in significantly increased mixing and noise radiation. In general, forcing the jet over a  $St_D$  range of 0.2 to 0.5 enhances mixing and increases jet noise (Bechert and Pfizenmaier 1975; Ahuja et al. 1982).

The high amplitude and bandwidth plasma actuators under development in the current work will enable us to explore forcing various instability modes in high-speed and high Reynolds number jets.

## 1.2

### Longitudinal vorticity generation

As was discussed, a major problem with forcing the shear layer instabilities in high-speed and high Reynolds number jets has been the lack of availability of high bandwidth and high amplitude actuators. For example, the shear layer instability frequency in a typical small-scale high subsonic jet in a laboratory is on the order of tens of kHz. On the other hand, imparting streamwise vorticity into the mixing layer of the jet through passive control techniques has been quite successful in both low- and high-speed and Reynolds number jets (e.g., Reeder and Samimy 1996; Hileman and Samimy 2003). Several techniques have been explored in the literature to generate streamwise vorticity. Small tabs, attached to the nozzle exit and used as streamwise vortex generators, were found to be effective devices in enhancing mixing and altering noise characteristics in both incompressible and compressible jets (e.g., Ahuja and Brown 1989; Samimy et al. 1993; Zaman et al. 1994; Reeder and Samimy 1996; Simonich et al. 2001; Hileman and Samimy 2003). Although the use of tabs or vortex generators of similar kind to enhance mixing is effective in both incompressible and compressible flows, it results in thrust losses due to the blockage effects (Zaman et al. 1994).

Chevrons, which are essentially tabs with less protrusion into the flow (i.e., gentler tabs), are currently being used in industry instead of tabs to reduce this thrust loss (Saiyed et al. 2003). Chevrons generate weaker streamwise vortices than tabs due to reduced penetration into the flow and cause less thrust loss at the expense of lower mixing enhancement and noise alteration than could be achieved with tabs. If one could generate the effects of tabs and

chevrons with an “on-command” actuator, the thrust loss could be minimized. For example, one could use it at take-off, where a major noise reduction is required, but deactivate it during cruise to minimize the thrust loss.

Zaman et al. (1994) explored streamwise vorticity generation mechanism by tabs and concluded that the main source of streamwise vorticity was the spanwise pressure gradient set up in front of the tab. Since a tab protrudes into the flow, it generates a spanwise pressure gradient regardless of whether the flow is subsonic or supersonic. In addition to the induced spanwise pressure gradient and thus streamwise vorticity, a tab generates a streamwise pressure gradient in front of the tab (Zaman et al. 1994) and thus spanwise vorticity. The governing equation is:

$$\frac{\partial p}{\partial x_i} = \mu \varepsilon_{ijk} \frac{\partial \omega_j}{\partial x_k} \quad (1)$$

which relates the spanwise and streamwise pressure gradients to streamwise and spanwise vorticity with the following equations:

$$\frac{\partial p}{\partial z} = \mu \frac{\partial \omega_x}{\partial y} \quad (2)$$

and

$$\frac{\partial p}{\partial x} = -\mu \frac{\partial \omega_z}{\partial y} \quad (3)$$

While production of streamwise vorticity by tabs has been reported by many researchers, only very recently Hileman and Samimy (2003) have reported the development of robust spanwise vorticity due to tabs in high-speed jets.

Kim and Samimy (1999) explored a streamwise vorticity generation mechanism by nozzle trailing edge cutouts that did not protrude into the flow. They concluded that the mechanism is still a spanwise pressure gradient, which is very small in subsonic jets and heavily depends on the flow regime in supersonic jets. A strong dependency of the rate of jet mixing and thus noise radiation on the nature of the trailing edge modifications has also been reported (Kerechanin et al. 2001). In recent years, small steady jets, termed micro jets, operating in underexpanded flow regime, have been distributed around and used to control supersonic impinging jets (Alvi et al. 2000; Lou et al. 2002). The control mechanism seems to be streamwise vorticity generated by the micro jets (Lou et al. 2002). Most recently Arakeri et al. (2003) forced a Mach 0.9 jet with micro jets and showed significant reduction in turbulence intensities. They attributed this effect to the change in the mean velocity profile and thus change in the initial instability of the mixing layer.

Plasma actuators under development in the current work are located just upstream of the exit of the nozzle. They could be configured to generate azimuthal (spanwise) and streamwise pressure gradients that mimic tabs or chevrons. Since these actuators could be powered at any frequencies (DC to 10's of kHz), they could also be used potentially to combine the effects of streamwise vorticity

with shear layer instability forcing to improve their overall effectiveness.

### 1.3

#### Plasma actuators

In recent years, there has been considerable interest in the use of electric discharge plasmas for flow control. The work in this field covers a wide range of specific experimental approaches and engineering applications. In particular, various methods of plasma generation, including DC, AC, RF, microwave, arc, corona, and spark electric discharges, as well as laser-induced breakdown, have been used to modify both subsonic and supersonic flow fields. These plasma configurations include both surface and volume-filling discharges sustained both at low and high gas temperatures. Engineering applications of the plasma-assisted flow control mainly focus on viscous drag reduction and control of boundary layer separation in subsonic flows (Roth et al. 2000; Corke and Matlis 2000; Artana et al. 2001; Leonov et al. 2001; Post and Corke 2003), shock wave modification and wave drag reduction in supersonic and hypersonic flows (Tret'yakov et al. 1996; Minucci et al. 2000; Bobashev et al. 2000; Adelgren et al. 2001; Yano et al. 1999; Adamovich 2001; Merriman et al. 2001; Leonov et al. 2002), jet or shear layer excitation (Troutt and McLaughlin 1982; Martens et al. 1996; Adelgren et al. 2002), and sound attenuation (Stepaniuk et al. 2003).

It is known that intense, localized, rapid heating produced by plasmas in high-current pulsed electric discharges and pulsed optical discharges produces strong shock waves, which can considerably modify the supersonic flow over blunt bodies and in supersonic inlets (Minucci et al. 2000; Bobashev et al. 2000; Adelgren et al. 2001). Basically, rapid near-adiabatic heating results in an abrupt pressure jump through the current filament.

The approach taken in this work is fundamentally different from the previously used glow discharge based supersonic flow control methods (Martens et al. 1996; Merriman et al. 2000). In the previous research, spatially distributed heating induced by AC or RF glow discharges were used to produce weak disturbances in the supersonic shear layer (Martens et al. 1996) or to weaken the oblique shock in the supersonic inviscid core flow (Merriman et al. 2000). These experiments were conducted at fairly low static pressures (i.e., at stagnation pressures of 0.3–1.0 atm and Mach numbers of 2.0–4.0). This allowed initiating and sustaining diffuse glow discharges, which weakly affected relatively large areas of the flow. In contrast, the main objective of the current research is to produce strong localized perturbations in high-pressure transonic and supersonic flows (at static pressures near 1 atm). This is achieved by a very rapid localized heating of the flow by a high-current filament formed by constriction of an electric discharge occurring at high pressures. Therefore the resultant localized pressure perturbations would act in a similar manner to a solid obstacle such as a tab suddenly placed in the flow. Repetitive pulsing of the discharge would enable control over the “obstacles” (i.e., pressure perturbations) and the frequency with which the plasma fires could be set to work with the instabilities of the jet to modify its properties.

The principal difference of the present approach from the glow discharge plasma flow control method developed by Roth et al. and Corke et al. is that it primarily relies on the arc plasma serving as a localized heating source. Such localized rapid flow heating is capable of producing significant local pressure perturbations (Leonov et al. 2002), which act as obstacles in the high-speed flow, thereby modifying the flow field. On the other hand, the glow discharge plasma flow control method is based on the direct flow entrainment by collisions with the charged species (ions) accelerated by the applied electric field. The feasibility of this method, which uses diffuse low-temperature plasmas sustained near solid surfaces, has been demonstrated at relatively low flow velocities (of the order of a few meters per second).

## 2 Experimental facilities and techniques

The experiments were conducted in the jet facility within the optically accessible anechoic chamber of the Gas Dynamics and Turbulence Laboratory (GDTL) at Ohio State University. The facility allows for easy optical access and simultaneous acoustic measurements with flow diagnostics. A brief description of the jet facility, flow visualizations set up, and plasma actuators will be given in this section.

### 2.1

#### Jet facility

In the current experiments, both axisymmetric and rectangular jets were used. The axisymmetric jets under study were created by a converging nozzle and a converging–diverging (c–d) nozzle with a design Mach number of 1.3. The converging nozzle was operated at Mach 0.9 and the c–d nozzle was operated at the fully expanded flow regime. The axisymmetric nozzles had an exit diameter of 25.4 mm (1 inch). The rectangular nozzle had a Mach number of 1.3 and an aspect ratio of 3 (1.27 cm × 3.81 cm). The inner contours of the supersonic nozzles were determined by the method of characteristics for uniform flow at the exit. The Reynolds numbers based on the jet diameter for Mach 0.9 and Mach 1.3 jets were  $6 \times 10^5$  and  $1 \times 10^6$ , respectively, and for the rectangular jet based on the jet height was  $5 \times 10^5$ .

The air for the jet was supplied by a four stage compressor; it was filtered, dried, and stored in two cylindrical tanks with a total capacity of 42.5 m<sup>3</sup> at a pressure of 16.5 MPa (1,600 ft<sup>3</sup> at 2,500 psi). A stagnation chamber was used to condition the jet air before exhausting it through the nozzle.

### 2.2

#### Measurement techniques

Two sets of results will be presented in this work. The first set details the characteristics of the plasma arc using current and voltage measurements and the resulting power used by the actuators. The second set presents and discusses flow visualization results demonstrating the plasma actuator's ability to increase mixing within the jet.

The current and voltage measurements of the plasma actuators were carried out using a Tektronix P6015A

high voltage probe and a Tektronix AM503S wide frequency range (DC-100 MHz) current probe. These data are presented in traces over a short time duration, but they are typical of what was observed at any given time. Additional details of the measurements will be given in the next section.

For flow visualization, the beam from a commercial 10 Hz pulsed Nd:YAG laser operating at 532 nm wavelength was formed into a sheet and directed through various optics to illuminate a cross-section of the jet. The laser was located outside of the chamber and the beam from the laser was directed into the chamber through a 2.5 cm hole in one of the large structural beams of the anechoic chamber. A framework connected to the ceiling of the anechoic chamber held the optical components used to create the laser sheet. A Princeton Instruments ICCD camera, placed outside of the chamber at an angle of approximately  $50^\circ$  to the laser sheet, captured cross-stream images of the jet. The camera had visual access to the jet flow via a removed wedge block on the anechoic chamber wall. The camera was placed behind the jet to prevent the plasma from being in the camera's field of view and the image acquisition system (camera and computer) had to be placed a large distance (over 4 m) away from the plasma to prevent electromagnetic interference with the image acquisition. Seeding for laser light scattering was provided using product formation where moisture contained in the warm, moist ambient air condensed upon entrainment into the mixing layer of the cold, dry jet.

### 2.3

#### Localized arc filament plasma actuators (LAFPA)

Figure 1 shows a schematic of the actuator arrangement in the axisymmetric nozzle extension. The 1.27 cm (0.5 inch) thick ceramic nozzle extension attached to an axisymmetric Mach 0.9 or 1.3 nozzle and a similar extension was used for the Mach 1.3 rectangular nozzle. In the present experiments, the extensions were made of either Macor or boron nitride machinable ceramic. Threaded copper electrodes, 2 mm in diameter, were placed in tapped holes of the nozzle extension flush with the inside wall, as shown in the figure. The distance between the adjacent electrodes was 4 mm in the current experiments. Every pair of electrodes constituted a localized plasma actuator powered by a variable frequency (2–100 kHz) high voltage PowerMax 3 kW AC power supply, which produced an arc filament discharge between the electrodes. With the power supplies used for these experiments, two actuators could be powered at any frequency and four actuators could be powered over a limited band of frequencies. An effort is underway to extend these capabilities to enable simultaneous powering of up to 8 actuators distributed around the jet and operating in phase or different phases. This is important for both streamwise vorticity generation and jet instability excitation.

The schematic of the electrical circuits are also shown in Fig. 1. The AC power supply consists of two 1,500 W amplifiers connected to a two-arm step-up high voltage transformer. The midpoint of the transformer output is grounded while the two high voltage outputs generate

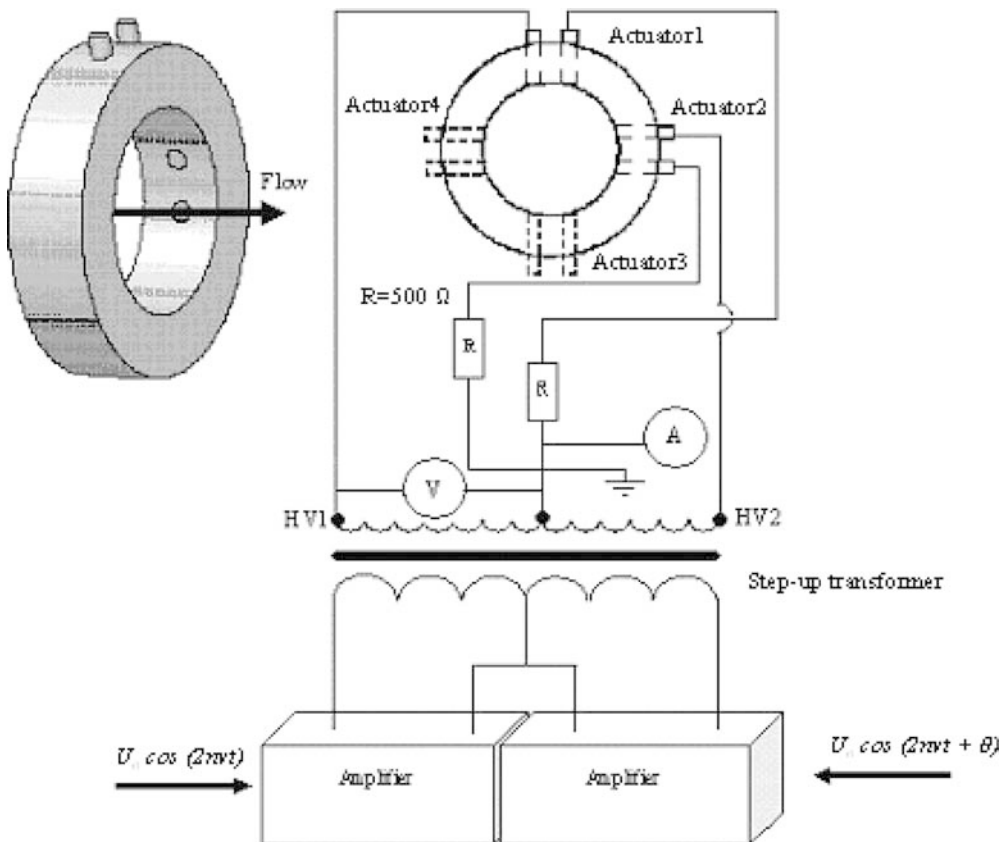


Fig. 1. Schematic of an axisymmetric nozzle extension with plasma actuators and their electrical circuit

signals  $180^\circ$  out of phase. The 1–10 V peak-to-peak sine wave input to the amplifiers is supplied by a function generator. A 500  $\Omega$  ballast resistor is connected in series on the ground side of every actuator. The locations for the measurement of the current and voltage are shown in the figure with a circled A and V, respectively.

As will be discussed in the experimental results, one problem encountered during these experiments was material ablation in between the electrodes (around arc filaments). The erosion occurred because of high temperatures produced in the plasma arc during operation. Several materials were used over the course of the experiments. Boron nitride was found to be the superior material for the actuator nozzle extension since it experienced essentially zero erosion (even with long run times of 30–60 s at a time). This is quite different from zirconium phosphate, another material we used for the nozzle extension, which was quite spectacular in the destruction caused by the plasma arc. As soon as the plasma was initiated within the zirconium phosphate nozzle extension, there was considerable material ablation as evidenced by small, red-hot, glowing chunks of the nozzle being blown downstream by the jet. The Macor nozzle extensions also had erosion between the actuator electrodes after short duration run times, but this was minor in comparison to that observed with zirconium phosphate.

### 3 Experimental results and discussion

This work is ongoing and in its infancy. As such, the results presented in this section are of a preliminary nature. However, it was deemed important to disseminate what has been learned on this important topic. Results that characterize the actuators (Sect. 3.1) and flow visualization images (Sect. 3.2) that show the effect of LAFPA forcing are presented. We initially used Macor for the nozzle extensions and obtained actuator characteristics and flow visualizations in both ideally expanded Mach 1.3 axisymmetric and rectangular jets. However, the actuator characteristics changed over time due to material ablation, so we will not present any actuator characterization results for the Macor extension. Flow visualizations will be presented for this extension since there was a direct comparison between the forced and the baseline cases where the baseline case includes the effect of material ablation.

Due to the problems associated with material ablation, further material searches were conducted, and these led us to the use of boron nitride for the nozzle extension material. Unlike the Macor extension, boron nitride was able to withstand the high thermal stresses imposed by the plasma arc. The use of boron nitride allowed for the characterization of the LAFPA, since the surface between the electrodes did not erode regardless of how many times they were used and the duration of the experiments. The LAFPA characterizations for the boron nitride nozzle along with a discussion of the use of a groove to stabilize the LAFPA in the jet are presented in Sect. 3.1. This is followed by flow visualization results using the Macor extension in Sect. 3.2.

### 3.1 Actuator characterization

As mentioned earlier, Macor extensions eroded considerably between the LAFPA electrodes, which caused the actuator characteristics to change over time. Thus, a reliable characterization of the LAFPA was only possible with the boron nitride extension. Figure 2 shows time-dependent voltage, current, and power in the AC discharge in a boron nitride nozzle extension without flow (i.e., in air at a static atmospheric pressure). Figure 1 shows the measurement locations for the current and voltage. The input AC voltage frequency for these results is  $\nu = 10$  kHz, while the forcing frequency (i.e., the frequency of periodic heating of the gas by the discharge) is expected to be  $f = 20$  kHz, since the plasma will fire on both the positive and negative cycles of the sinusoidal input voltage. The top power trace (shown as Input Power) shows the output from the high-voltage AC power supply (it is simply the product of the current and voltage traces). The bottom power trace (shown as Power Across Plasma) shows the amount of power,  $P$ , imparted into the flow by the plasma, which is determined from:  $P = I(V - IR_B)$ , where  $I$  and  $V$  are the measured current and voltage given in the figure, and  $R_B$  is the ballast resistance (500  $\Omega$ ). From Fig. 2 one can see that the peak power supply voltages in the discharge are quite low, only about 300 V, although much higher voltages of up to several kilovolts are needed to produce initial breakdown between the electrodes of either 4 mm or 8 mm separation. After breakdown, the discharge voltage drops as the plasma conductivity increases and reaches quasi steady-state. At these conditions, the maximum current between the electrodes,  $\sim 0.25$  A, is limited mainly by the ballast resistor. These currents and voltages indicate that a continuous arc discharge is being sustained between the electrodes. The peak power generated by the power supply and the peak power consumed in the plasma arc are quite low, 60–70 W and 30–50 W, respectively. The time-averaged powers at these conditions are 38 W and 19 W, respectively.

The LAFPA characteristics while operating within an axisymmetric, Mach 0.9 jet flow are shown in Fig. 3. The static pressure at the actuator location is 1 atm. One can see that the flow completely changes the discharge behavior. In particular, the peak currents and voltages become much higher, up to 2 kV and 0.6 A, respectively. The high-amplitude voltage spike at the beginning of every AC half-period indicates that breakdown is initiated and plasma is indeed generated at the forcing frequency of 20 kHz instead of at the input frequency of 10 kHz. In addition, there are well-pronounced and quite regular current and voltage oscillations within every AC period. The power trace has regular spikes separated by a period of 0.05 ms (20 kHz frequency). There are also several smaller peaks that occur after each large spike (these are separated by  $\sim 6$   $\mu$ s). At these conditions, the peak power (amplitude between 500 and 800 W) is reached at the moment of breakdown at the beginning of every AC half-period, when both the applied voltage and the current are at their maximum levels. After breakdown, the time-dependent power does not exceed 300 W. The

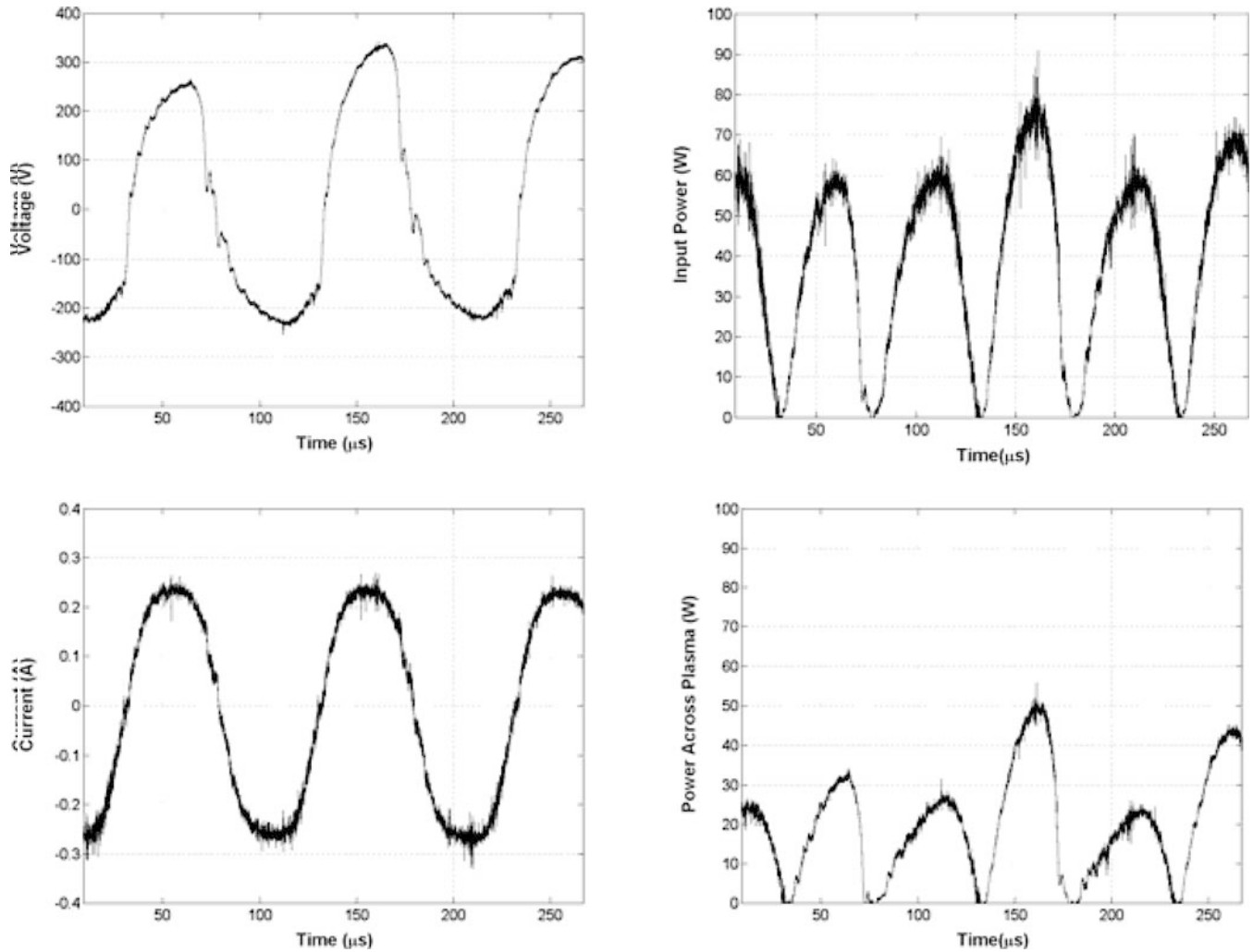


Fig. 2. Voltage, current, and power traces in the plasma actuator.  $v = 10$  kHz,  $f = 20$  kHz, boron nitride axisymmetric nozzle, no-flow. The AC amplifier input signal intensity is 5 V peak-to-peak

time-averaged plasma power at these conditions (114 W and 78 W) is considerably higher than without the flow (38 W and 19 W) for the total power and power imparted into the flow, respectively. However, these actuator powers are still small compared to the power of the Mach 0.9 jet (at 1 atm exit pressure and the mass flow rate of 0.2 kg/s,  $\frac{1}{2}\dot{m}u^2 = 8.3$  kW). These results demonstrate that the actuator power is only about 1% of the flow power. This power consumption can be reduced considerably, as will be discussed below.

The oscillations between the spikes in the traces of Fig. 3 might be *qualitatively* explained by stretching of plasma by the flow and “restarting” between the electrodes. Figure 4 shows a *cartoon* of the process believed to be involved. A short segment of the time traces are shown with a schematic to elucidate the conjectured process. The initial plasma firing coincides with the large voltage spike (event 1 in the schematic). Subsequently, the plasma has formed and the gap resistance is low (event 2). The initial plasma arc is carried downstream by the flow causing the gap resistance to increase. During some experiments, one can clearly see the plasma arc being stretched downstream by the flow. Once the gap resistance becomes sufficiently

high due to the plasma arc being stretched downstream, a new arc is established between the filaments (event 3). Once the new arc is created, the stretched plasma arc decays (i.e., the arc that had blown downstream dissipates) (event 4). This process of stretching and re-arcing would repeat at a rate matching the oscillations in the power trace. With an approximate exit velocity of 290 m/s for the Mach 0.9 jet, a 6  $\mu$ s time separation corresponds to a distance of 1.7 mm, which would correspond to the stretched length of the filament.

Machining a simple groove ring right before the nozzle extension exit and imbedding the electrodes within the groove reduced the anomalies that were observed in the previous results that were attributed to the plasma stretching. Figure 5 shows the actuator characteristics that were obtained from a plasma arc that was created from a boron nitride extension that had a 1 mm deep, 1.5 mm wide groove ring (the groove encompassed the jet circumference) within the same Mach 0.9 jet. The electrodes were located in the groove trough. Comparing these results with those without a groove (Fig. 4), it is clear that setting the electrodes in the groove removes the breakdown voltage spikes and considerably reduces the amplitude of

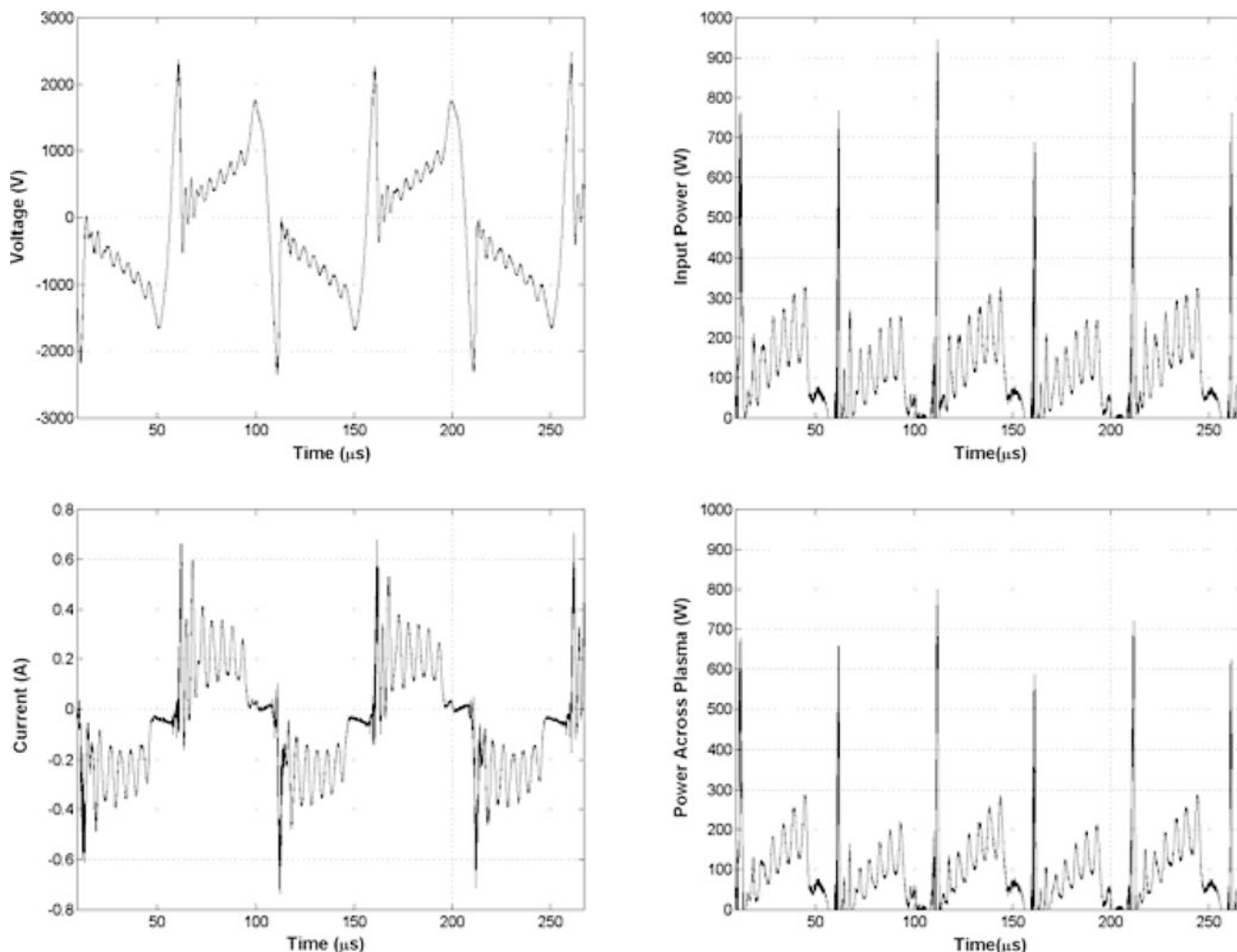


Fig. 3. Voltage, current, and power traces in a plasma actuator,  $\nu = 10$  kHz,  $f = 20$  kHz, boron nitride axisymmetric nozzle, Mach 0.9 jet. The AC amplifier input signal intensity is 5 V peak-to-peak

the oscillations that were observed in the voltage and current traces. This is especially true for the current trace, which now resembles the sinusoid of the plasma arc in the no-flow case (Fig. 2). The absence of the breakdown spikes demonstrates that the plasma is not blown off by the flow when the AC voltage is at minimum, while reduction of the current oscillations within the period suggests that the plasma stretching schematically shown in Fig. 4 is greatly reduced. Basically, in this case the plasma is “shielded” and stabilized by the groove. This results in a more regular time-dependent power variation, which becomes nearly harmonic. This stabilization was observed visually as the plasma did not stretch downstream of the nozzle exit when there was a groove surrounding the plasma arc. It also adds validity to the conjecture described in the previous paragraph and Fig. 4.

Similar plasma behavior was observed at higher input frequencies as well, but both peak voltage and peak current values are somewhat reduced, as well as the time-averaged power (24 W total and 20 W imparted into the flow at  $\nu = 30$  kHz). Qualitatively, this occurs because the voltage spikes become more frequent, so that the

plasma is not completely decayed (or removed by the flow) between the voltage maxima. Also, at higher frequencies breakdowns occur only during negative voltage spikes, which make the voltage and current pulses polarity-dependent. As a result, the forcing frequency, instead of being twice the input AC frequency, becomes equal to the input AC frequency. Note that voltage, current, and power spikes during periodic breakdowns do not significantly contribute to the time-averaged power. As was observed at the lower input frequency, adding the groove stabilizes the plasma, removes periodic breakdowns and makes the power profile more regular. Also, the remaining high-frequency oscillations can be reduced by increasing the input AC power. This was shown by operating the actuator at an AC input frequency of 10 kHz and at two different AC amplifier input voltages of 3 V peak-to-peak and 6 V peak-to-peak. Clearly, raising the input voltage results in higher power imparted into the flow (the output power at the plasma was increased from 34 W to 46 W), but also shows that the number of sharp spikes drops considerably with increased input power.

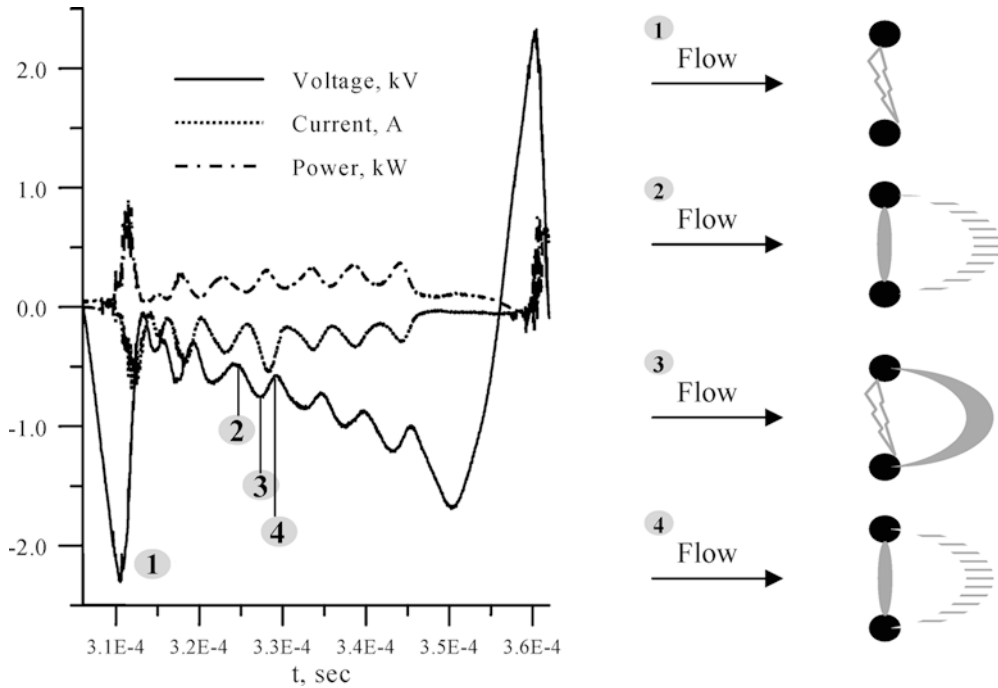


Fig. 4. Cartoon of the plasma stretching effect on the discharge voltage and current

As was discussed earlier, these actuators could be distributed around the jet and operated at different phases to force various azimuthal modes of the jet. Figure 6 shows current traces of two actuators operating  $90^\circ$  out of phase, which demonstrates such potential of the LAFPA.

Time-averaged power calculations based on the discharge current and voltage measurements at different input frequencies ( $\nu$  from 1 to 40 kHz) show a general trend of power reduction as the frequency increases (see Fig. 7). The power consumption for the actuators imbedded within a ring groove is much lower than the case without a groove in lower frequencies, but comparable in higher frequencies—the power in both cases at frequencies above 30 kHz approaches that of the no-flow case. Again, for input frequencies greater than 10 kHz ( $\nu \geq 10$  kHz), the actuator power is much less than 1% of the flow power. Although much work remains in the optimization of the LAFPA, these results demonstrate the feasibility of energy-efficient operation of localized arc plasma actuators, with straightforward control of their amplitude, frequency, and phase.

### 3.2

#### Flow visualization results

A series of flow visualization experiments were conducted with the Macor nozzle extensions. The experimental results, which are presented in this section, led to many of the improvements in the LAFPA design. As discussed earlier, the plasma gradually eroded the nozzle extension with this material. However, flow visualizations for the baseline cases were obtained right after the visualizations of the forced cases. Therefore the comparisons shown below are legitimate and validate the ability of plasma actuators to control high-speed and high Reynolds number flows. These limited results show the potential of the LAFPA for increasing mixing. The visualized jets of this section are from Mach 1.3 ideally expanded axisymmetric and rectangular jets.

Typical results for the Mach 1.3 rectangular jet are shown in Fig. 8. In these experiments, two pairs of electrodes (4 mm between each pair with a common ground electrode) lined up in the spanwise direction, were powered with an AC input voltage frequency,  $\nu = 10$  kHz, in phase with each other ( $\theta = 0^\circ$ ). While running the experiment, a small amount of material between the electrodes (around the arc filaments) was ablated due to thermal stresses and a small groove formed between the electrodes. This small groove proved useful as it stabilized the arcs, preventing them from being blown off by the jet flow. Since the arc was expected to be initiated twice during each period, in both positive and negative peak voltages, the forcing frequency,  $f$ , for an input frequency,  $\nu$ , of 10 kHz was expected to be 20 kHz. The figure shows four images, two average images (a and c) and two typical instantaneous images (b and d), of the jet with plasma off (baseline) and plasma on (forced). Each of the two average images is an average of 25 instantaneous (9 ns exposure time) images obtained at the pulsed Nd:YAG laser frequency of 10 Hz (total run time of 2.5 s). The laser pulses were not phase-locked with the AC input voltage due to plasma arc electromagnetic interference. The sheet of spanwise laser light passed orthogonal to the jet centerline at 8 jet heights (jet height,  $h=12.7$  mm) downstream of the nozzle/extension exit. The bright region in the images is the jet's mixing layer, which is illuminated via scattering of the laser light by condensed water particles in the mixing layer. These particles are generated by condensation of moisture in the entrained ambient air when it mixes with the cold and dry jet air.

The shape of a nearly rectangular mixing layer can be seen in the baseline images. The somewhat brighter bottom section of the mixing region in the average image is due to the flow perturbation by the erosion pit in the center of the bottom nozzle extension in between the electrodes, created by the hot arcs after multiple runs.



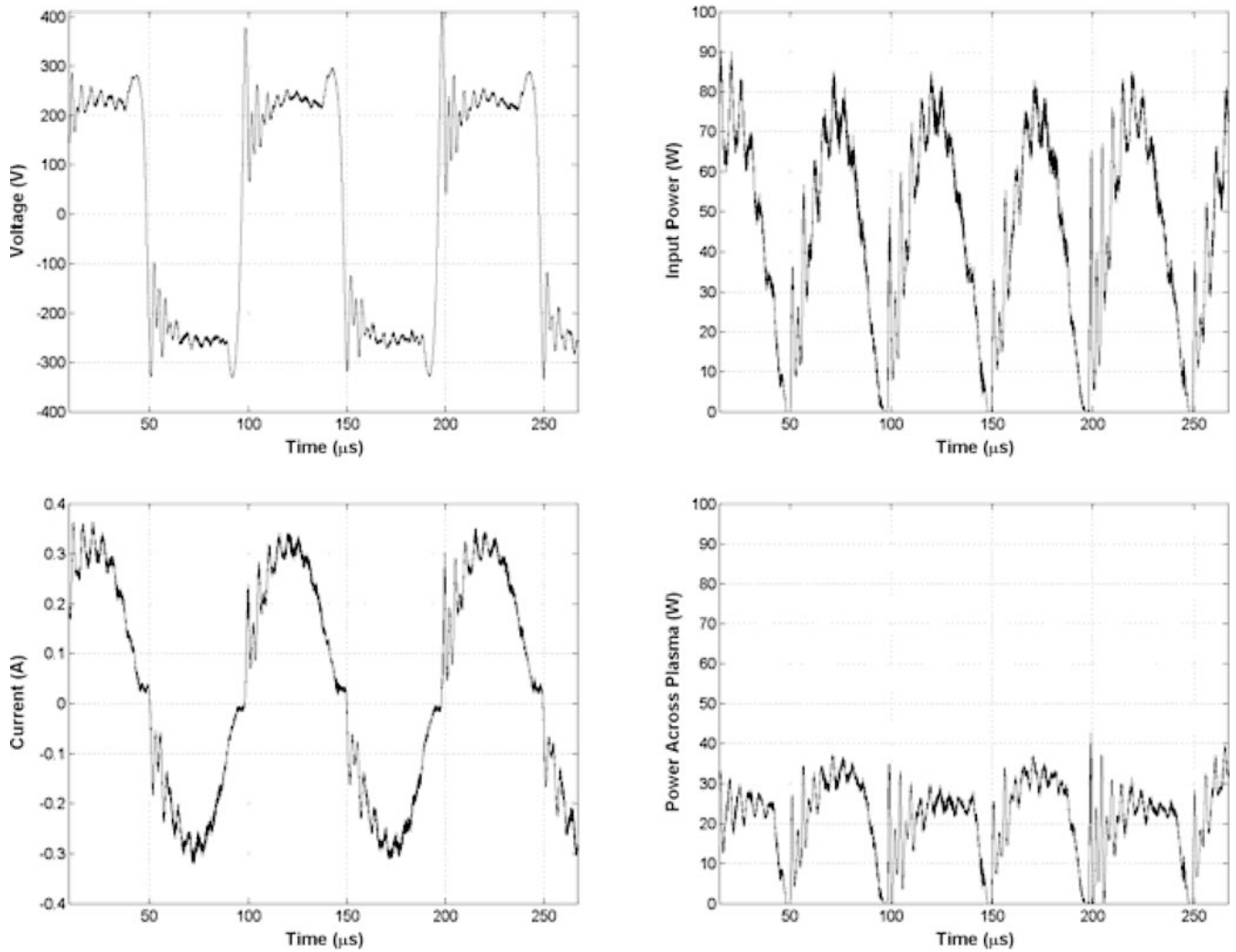


Fig. 5. Voltage, current, and power traces in the plasma actuator,  $\nu=10$  kHz,  $f=20$  kHz, boron nitride axisymmetric nozzle with a groove, Mach 0.9 jet. The AC amplifier input signal intensity is 5 V peak-to-peak

Apparently, the temperature in the arc exceeds the maximum operation temperature of the Macor extension, quoted as 1,000 °C by the manufacturer. When the plasma was turned on, the scattered light intensity in the lower part of the mixing layer dramatically increased (the actuator was located in the lower part of the nozzle). This implies significant increase in the amount of entrained ambient air within the mixing layer due to streamwise vorticity. Not only the increased entrainment but also the distorted shape of the jet cross-section (compare a with c and b with d), which is similar to a jet cross-section with a tab (Hileman and Samimy 2003), points to the existence of streamwise vortices in the forced case. These streamwise vortices cannot be directly visualized by the technique used here, as their cores are located outside of the mixing layer (Zaman et al. 1994).

Note that simply heating the flow would reduce condensation of ambient moisture within the jet's mixing layer and this would result in a decrease in mixing layer intensity; an increase in mixing layer intensity

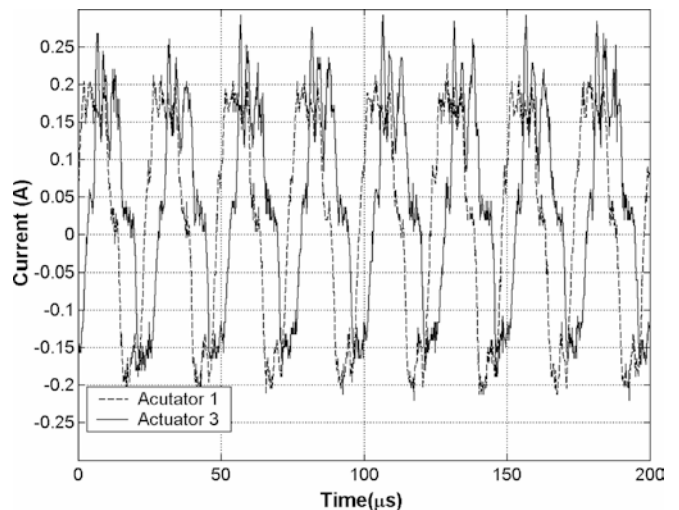


Fig. 6. Current traces for two actuators operating 90° out of phase

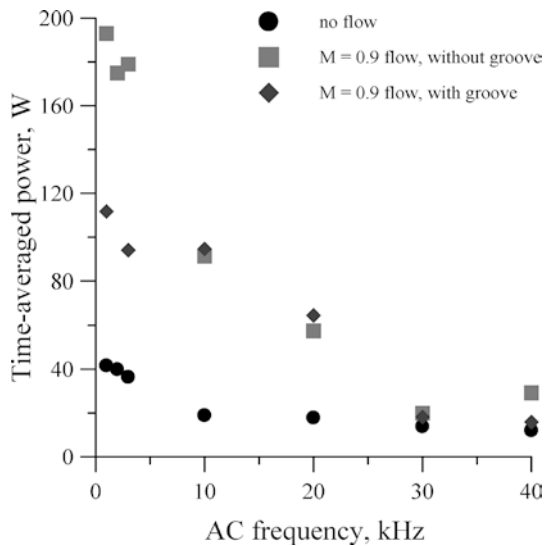


Fig. 7. Time-averaged actuator power as a function of the AC frequency for boron nitride nozzle extension. AC amplifier input signal intensity is 5 V peak-to-peak

demonstrates that the observed effect is indeed due to enhanced mixing via streamwise vortices, which are being induced by forcing. Similar effects were also observed when the forcing frequency was varied from 4 to 20 kHz.

The flow visualization results in an ideally expanded Mach 1.3, axisymmetric jet are shown in Fig. 9. The jet cross-sectional images were taken near the end of the potential core ( $6D$  downstream of the nozzle/extension exit;  $D$  is the nozzle exit diameter) and are the averages of 25 instantaneous images. The images shown in (a) and (c) are for the unforced jet (baseline) and those in (b) and (d) were taken with two LAFPA operating with an input frequency,  $\nu$  of 40 kHz, which gives a forcing frequency,  $f$ , of 80 kHz. In image (b), the actuators are located on the top and bottom (actuators 1 and 3 in Fig. 1,  $180^\circ$  apart azimuthally) while in image (d) they are located on the top and left (actuators 1 and 4 in Fig. 1,  $90^\circ$  apart azimuthally). Again, only the mixing region is visualized and the intensity of light in the mixing region is directly related to entrainment of the moist ambient air into the jet. It is obvious that the forcing has significantly increased mixing (ambient fluid entrainment) as shown by the increased

scattered light intensity throughout the cross-stream section of the shear layer in image (b) and in the fourth quadrant of (d). Note also the reduced average jet core size in the image in the former forced case.

A point of interest is that the two actuators for image (b) were operating with  $180^\circ$  phase difference (azimuthal mode,  $m = \pm 1$ ) while those in (d) were in phase. For two LAFPA operating on opposite sides of the nozzle, the most dramatic increase in mixing was achieved with input frequencies above 10 kHz (forcing frequency of 20 kHz) and a  $180^\circ$  phase difference. When two LAFPA were used in close proximity (d), the phase was not as important as shown by the increased mixing with  $0^\circ$  phase difference.

Results using two LAFPA at a forcing frequency of 80 kHz were presented since this produced the maximum mixing (as measured using flow visualization). The boundary layer velocity profile was measured right after the nozzle exit for Mach 0.9 jet (Kastner et al. 2003). The momentum thickness calculated using this profile was 0.08 mm, which put the initial shear layer instability frequency at 50–100 kHz ( $St_\theta = 0.01$ – $0.02$ ). The initial shear layer instability frequency for Mach 1.3 is even higher, as the boundary layer is thinner and much tougher to make any velocity measurements. Hence, the LAFPA was likely operating close to initial shear layer instability frequencies. The most results using these actuators in a Mach 1.3 ideally expanded axisymmetric jet are present in Samimy et al. (2004).

#### 4 Concluding remarks

The development and characterization of a class of high amplitude and bandwidth actuators, that we have termed ‘localized arc filament plasma actuators’, for high-speed and high Reynolds number jet control were presented. Preliminary flow visualizations results to evaluate actuators’ authority were also presented and discussed. The mechanism of LAFPA for flow control is local heating of the flow. An arc filament initiated between electrodes of the actuator in the flow generates rapid (on the time scale of a few microseconds) local heating up to high temperatures. The arc produces a local pressure rise and volume change adjacent to the surface of the nozzle in the flow. The arc filament can be generated from DC to very high frequencies, covering the entire range of jet column

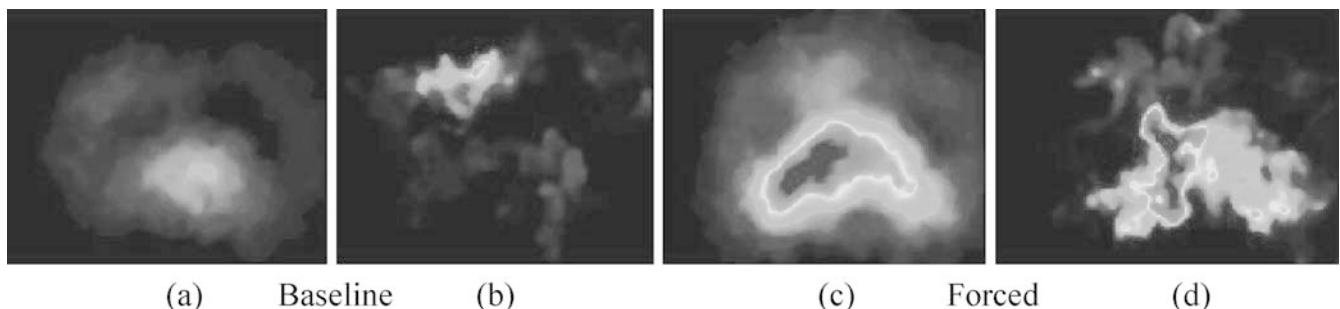


Fig. 8a–d. Cross-stream images of Mach 1.3 rectangular jet at 8 h downstream of the nozzle exit for the baseline (a) and (b) and for forcing with two adjacent 4-mm actuators with a common

ground electrode (8-mm between the farthest electrodes) and common phase (c) and (d),  $\nu = 10$  kHz,  $f = 20$  kHz. Images a and c are averages of 25 instantaneous images (b) and (d)

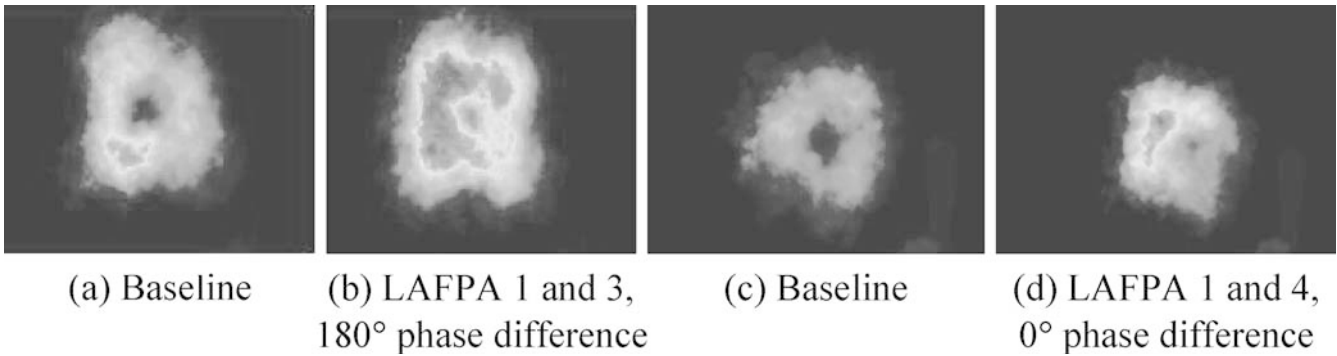


Fig. 9a–d. Cross-stream average images (taken at  $6D$ ) showing the effect of forcing on an axisymmetric, Mach 1.3, ideally expanded jet. Images a and c are baseline images. The jets in images b and d were forced with two LAFPA operating with  $\nu = 40$  kHz,

$f = 80$  kHz. The LAFPA in image b were located at azimuthal locations of  $0$  and  $180^\circ$  (top and bottom) and were operated with a  $180^\circ$  phase difference while those in image d were located at  $0$  and  $270^\circ$  (top and left side) and were operated in phase

and shear layer instabilities in even very small laboratory jets. Due to the nature of the LAFPA, it can be used potentially to perform two functions (either separately or in unison): streamwise vorticity generation in a manner similar to chevron/tabs and forcing the jet at any instability frequency within the jet.

Preliminary results have demonstrated the potential of LAFPA in generating streamwise vortices in a Mach 1.3, rectangular, ideally expanded jet by significantly affecting the jet flow field. Similar effects were observed in Mach 0.9 and 1.3 ideally expanded axisymmetric jets. We also demonstrated the range of forcing frequencies achievable with the LAFPA by forcing a Mach 1.3, axisymmetric jet at frequencies that extend from the jet column to the shear layer flow instability frequencies. While we have only used the LAFPA forcing over a limited number of Mach numbers and geometries due to time and resource constraints, there is no physical limitation in the application of LAFPA forcing. It could be used to create streamwise vortices or excite jet instabilities (such as the jet column or the shear layer instabilities). In addition, a phase lag can be imposed between the individual plasma arcs to force azimuthal modes within the jet. The LAFPA forcing can be applied to jets of any geometry or Mach number.

Clearly, these actuators have opened up opportunities in high-speed jet control technology that, prior to now, did not exist. The actuators could be developed into a variable frequency (up to 100 s of kHz) and high amplitude phased plasma actuator array (4–8 actuators). The array could then be employed in the exploration of various means of mixing enhancement and noise mitigation in high-speed jets with various Mach numbers.

While we tested the actuators in only cold jets, we expect them to be effective in heated jets as well. For example, exhaust jet temperature in a typical commercial aircraft would be on the order of 700–800 K. Although no arc temperature measurements were performed, Macor erosion indicates that the temperature of the arc plasma considerably exceeds the maximum operational temperature of the ceramic, which is about 1,250 K. This implies that the flow heating effect by the plasma should be rather substantial for flow temperatures up to 800 K (and perhaps higher as well).

## References

- Adamovich IV (2001) Control of electron recombination rate and electron density in optically pumped nonequilibrium plasmas. *J Phys D Appl Phys* 34:319–325
- Adelgren RG, Elliott GS, Knight D (2001) Energy deposition in supersonic flows. Am Inst Aeronaut Astronaut Paper 2001-0885
- Adelgren RG, Elliott GS, Crawford JB (2002) Axisymmetric jet shear layer excitation induced by electric arc discharge and focused laser energy deposition. Am Inst Aeronaut Astronaut Paper 2002-0729
- Ahuja KK, Lepicovsky J, Burrin RH (1982) Noise and flow structure of a tone-excited jet. Am Inst Aeronaut Astronaut J 20(12):1700–1706
- Ahuja KK, Brown WH (1989) Shear flow control by mechanical tabs. Am Inst Aeronaut Astronaut Paper 1989-0994
- Alvi FS, Elavarasan R, Shih C, Garg G, Krothapalli A (2000) Active control of supersonic impinging jets using microjets. Am Inst Aeronaut Astronaut Paper 2000-2236
- Arakeri VH, Krothapalli A, Siddavaram V, Alkisar MB, Lourenco LM (2003) On the use of microjets to suppress turbulence in a Mach 0.9 axisymmetric jet. *J Fluid Mech* 490:75–98
- Artana G, Adamo J, Léger L, Moreau E, Touchard G (2001) Flow control with electrohydrodynamic actuators. Am Inst Aeronaut Astronaut Paper 2001-0351
- Bechert D, Pfizenmaier E (1975) On the amplification of broad band jet noise by a pure tone excitation. *J Sound Vib* 43(3):581–587
- Bobashev SV, D'yakonova EA, Erofeev AV, Lapushikina TA, Maslennikov VG, Poniaev SA, Sacharov AA, Vasil'eva RV (2000) Shock-tube facility for MGD supersonic flow control. Am Inst Aeronaut Astronaut Paper 2000-2647
- Cohen J, Wygnanski I (1987) The evolution of instabilities in the axisymmetric jet, Part 1: The linear growth of disturbances near the nozzle. *J Fluid Mech* 176:191–219
- Corke TC, Matlis E (2000) Phased plasma arrays for unsteady flow control. Am Inst Aeronaut Astronaut Paper 2000-2323
- Crow SC, Champagne FH (1971) Orderly structure in jet turbulence. *J Fluid Mech* 48:547–591
- Gutmark E, Ho C-M (1983) Preferred modes and the spreading rate of jets. *Phys Fluids* 26(10):2932–2938
- Hileman J, Samimy M (2003) Effects of vortex generating tabs on noise sources in an ideally expanded Mach 1.3 Jet. *Int J Aeroacoustics* 2(1):35–63
- Ho C-M, Huerre P (1984) Perturbed free shear layers. *Ann Rev Fluid Mech* 16:365–424
- Kastner J, Hileman J, Samimy S (2004) Exploring high-speed axisymmetric jet noise control using hartmann tube fluidic actuators. Am Inst Aeronaut Astronaut Paper 2004-0186
- Kerechanin C, Samimy M, Kim J-H (2001) Effects of nozzle trailing edges on acoustic field of supersonic rectangular jet. Am Inst Aeronaut Astronaut J 39(6):1065
- Kibens V (1979) Discrete noise spectrum generated by an acoustically excited jet. Am Inst Aeronaut Astronaut J 18:434–451
- Kibens V, Dorris J III, Smith DM (1999) Active flow control technology transition: The Boeing ACE program. Am Inst Aeronaut Astronaut Paper 1999-3507

- Kim J-H, Samimy M (1999) Mixing enhancement via nozzle trailing edge modifications in a high-speed rectangular jet. *Phys Fluids* 11(9):2731
- Laufer J, Yen T-C (1983) Noise generation by a low-Mach-number jet. *J Fluid Mech* 134:1-31
- Leonov S, Biturin V, Kolesnichenko Y (2001) Dynamic of a single-electrode HF plasma filament in supersonic airflow. *Am Inst Aeronaut Astronaut Paper* 2001-0493
- Leonov S, Biturin V, Savelkin K, Yarantsev D (2002) Effect of electrical discharge on separation processes and shocks position in supersonic airflow. *Am Inst Aeronaut Astronaut Paper* 2002-0355
- Lepicovsky J, Brown WH (1987) Effects of nozzle-exit boundary-layer conditions on excitability of heated free jets. *Am Inst Aeronaut Astronaut Paper* 1987-2723
- Long DF, Kim H, Arndt REA (1985) Controlled suppression or amplification of turbulent jet noise. *Am Inst Aeronaut Astronaut J* 23(6):828-833
- Lou H, Alvi FS, Shih C, Choi J, Annaswamy A (2002) Active control of supersonic impinging jets: Flowfield properties and closed-loop strategies. *Am Inst Aeronaut Astronaut Paper* 2002-2728
- Martens S, Kinzie KW, McLaughlin DK (1996) Structure of coherent instabilities in a supersonic shear layer. *Am Inst Aeronaut Astronaut J* 34(8):1555
- Merriman S, Ploenjes E, Palm P, Adamovich IV (2000) Shock wave control by nonequilibrium plasmas in cold supersonic gas flows. *Am Inst Aeronaut Astronaut Paper* 2000-2327
- Merriman S, Christian A, Meyer R, Kowalczyk B, Palm P, Adamovich IV (2001) Studies of conical shock modification by nonequilibrium RF discharge plasma. *Am Inst Aeronaut Astronaut Paper* 2001-0347
- Michalke A (1965) On spatially growing disturbances in an inviscid shear layer. *J Fluid Mech* 23:521-544
- Minucci MAS, Bracken RM, Myrabo LN, Nagamatsu HT, Shanahan KJ (2000) Experimental investigation of an electric arc simulated 'air spike' in hypersonic flow. *Am Inst Aeronaut Astronaut Paper* 2000-0715
- Parekh DE, Kibens V, Glezer A, Wiltse JM, Smith DM (1996) Innovative jet flow control: Mixing enhancement experiments. *Am Inst Aeronaut Astronaut Paper* 1996-0308
- Post ML, Corke TC (2003) Separation control on high angle of attack airfoil using plasma actuators. *Am Inst Aeronaut Astronaut Paper* 2003-1024
- Reeder MF, Samimy M (1996) The evolution of a jet with vortex-generating tabs: Real-time visualization and quantitative measurements. *J Fluid Mech* 311:73
- Reynolds WC, Parekh DE, Juvet PJD, Lee MJD (2003) Bifurcating and blooming jets. *Annu Rev Fluid Mech* 35:295-315
- Roth JR, Sherman DM, Wilkinson SP (2000) Electrohydrodynamic flow control with a glow-discharge surface plasma. *Am Inst Aeronaut Astronaut J* 38(7):1166-1172
- Samimy M, Zaman KBMQ, Reeder MF (1993) Effect of tabs on the flow and noise field of an axisymmetric jet. *Am Inst Aeronaut Astronaut J* 31:609
- Samimy M, Adamovich I, Kim J-H, Webb B, Keshav S, Utkin Y (2004) Active control of high-speed jets using localized arc filament plasma actuators. *Am Inst Aeronaut Astronaut Paper* 2004-2130
- Saiyed NH, Mikkelsen KL, Bridges JE (2003) Acoustics and thrust of quiet separate-flow high-bypass-ratio nozzles. *Am Inst Aeronaut Astronaut J* 41(3):372-378
- Simonich JC, Narayanan S, Barber TJ, Nishimura, M (2001) Aeroacoustic characterization noise reduction and dimensional scaling effects of high subsonic jets. *Am Inst Aeronaut Astronaut J* 39(11):2062-2069
- Stepaniuk V, Sheverev V, Ötügen MV, Tarau C (2003) Sound attenuation by glow discharge plasma. *Am Inst Aeronaut Astronaut Paper* 2003-0371
- Tret'yakov PK, Garanin AF, Grachev GN, Krainev VL, Ponomarenko AG, Tischenko VN, Yakovlev VI (1996) Control of supersonic flow around bodies by means of high-power recurrent optical breakdown. *Phys Doklady* 41(11):566
- Troutt TR, McLaughlin DK (1982) Experiments on the flow and acoustic properties of a moderate Reynolds number supersonic jet. *J Fluid Mech* 116:123-156
- Yano R, Aithal SM, Subramaniam VV, Contini V, Palm P, Merriman S, Adamovich I, Lempert W, Rich JW (1999) Experimental characterization of shock dispersions in weakly ionized nonequilibrium plasmas. *Am Inst Aeronaut Astronaut Paper* 1999-3671
- Zaman KBMQ, Hussain AKMF (1981) Turbulence suppression in free shear flows by controlled excitation. *J Fluid Mech* 103:133-159
- Zaman KBMQ, Samimy M, Reeder MF (1994) Control of an axisymmetric jet using vortex generators. *Phys Fluids* 6:778